ADVANCED ENERGY MATERIALS
www.advenergymat.de

Triboelectric Nanogenerator for Sustainable Wastewater Treatment via a Self-Powered Electrochemical Process

Shuwen Chen, Ning Wang, Long Ma, Tao Li, Magnus Willander, Yang Jie, Xia Cao, and Zhong Lin Wang**

By harvesting the flowing kinetic energy of water using a rotating triboelectric nanogenerator (R-TENG), this study demonstrates a self-powered wastewater treatment system that simultaneously removes rhodamine B (RhB) and copper ions through an advanced electrochemical unit. With the electricity generated by R-TENG, the removal efficiency (RE) of RhB can reach the vicinity of 100% within just 15 min when the initial concentration of RhB is around 100 ppm at optimized conditions. The removal efficiency of copper ions can reach 97.3% after 3 h within an initial concentration of 150 ppm at an optimized condition. Importantly, a better performance and higher treating efficiency are found by using the pulsed output of R-TENG than those using direct current (DC) supply for pollutant removal when consuming equal amount of energy. The recovered copper layer on the cathode through R-TENG is much denser, more uniform, and with smaller grain size (d = 20 nm) than those produced by DC process, which also hints at very promising applications of the R-TENG in electroplating industry. In light of the merits such as easy portability, low cost, and effectiveness, this R-TENG-based self-powered electrochemical system holds great potential in wastewater treatment and electroplating industry.

1. Introduction

Water pollution and energy scarcity pose great challenges to human and become two of the most pressing global issues. However, tackling these problems is still very tough even with likely improvements in efficiency and environmental conservation.[1] The horrendous work, the complexity of pollutants, and the superior difficulty of treating refractory pollutants make wastewater treatment rather difficult and energy intensive. Thus, developing green and cost-effective wastewater treatment method is very important for balancing the tradeoff between electricity supply from fossil fuels and long-term preservation of natural resources.[2]

Nowadays, techniques for wastewater treatment include advanced oxidation processes (AOPs),[3] biological treatment,[4,5] physico-chemical methods,[6] enzymatic decomposition,[7] and electrochemical methods.[8] Among these techniques, electrochemical technologies have gained increased interest for its versatility, environmental compatibility, potential cost, and higher effectiveness even for refractory pollutants such as dyes and metals.[9] However, its practical industrial applications are still restricted by the very high energy consumption, and so it is with another electrochemical industry, electroplating. The latter consumes electric power to reduce dissolved metal cations and form a coherent metal coating on an electrode.[10]

To solve these problems of high energy consumption during electrochemical wastewater treatment and make it a sustainable process, only microbial fuel cell (MFC)[4,11] has been proposed as far as we know. However, the flowing kinetic energy of wastewater which harbors great energy,[12] has rarely been harvested for sustainable and self-driven wastewater treatment. Recently, we first proposed a self-powered electrical process using the energy directly harvested from the environment for splitting water,[12] desalinating seawater,[13] and cleaning air pollutants.[14]

Herein, we fabricated a self-powered multi-functional system, which not only electrochemically removes rhodamine B (RhB) and copper ions in wastewater but also simultaneously accomplishes metal electrodeposition by using the energy harvested from the flowing kinetic energy of wastewater through an R-TENG.[15] When the R-TENG rotates at a speed of 600 rpm, the system could remove almost 100% of the RhB just within 15 min

S. Chen, T. Li, Prof. M. Willander, Prof. X. Cao, Prof. Z. L. Wang
Beijing Institute of Nanoenergy and Nanosystems
Chinese Academy of Sciences
National Center for Nanoscience and Technology
Beijing 100083, P. R. China
E-mail: caoxia@binn.cas.cn
Prof. N. Wang
School of Chemistry and Environment
Beihang University
Beijing 100083, China
L. Ma
Wuhan Mechanical Technology College
Wuhan 430075, China
Y. Jie, Prof. X. Cao
School of Chemistry and Biological engineering
University of Science and Technology Beijing
Beijing 100069, China
Prof. Z. L. Wang
School of Material Science and Engineering
Georgia Institute of Technology
Atlanta, GA 30332-0245, USA
E-mail: zlwang@gatech.edu

DOI: 10.1002/aenm.201501778

(under initial concentration below 100 ppm) and 97.3% of the Cu^{2+} for 3 h (under initial Cu^{2+} concentration about 150 ppm). What is noteworthy is RhB can hardly be detected after treatment, which is much better than those driven by direct current (DC) supply, indicating its high efficiency of the system driven by R-TENG for treating organic pollutants with low concentrations. Besides treating wastewater, we also found that the recovered copper crystals on the cathode through R-TENG is much denser, more uniform and with smaller grain size than those produced by DC process. Such a high-quality deposition process makes the R-TENG-based system also very promising for electroplating. With a collection of compelling features, such as high removal efficiency for RhB and copper ions, feasibility for organic pollutants with low concentration, extremely low cost, simplicity, and reusability, the presented work not only provides a new and efficient pathway for sustainable wastewater treatment, but also provides access to other self-powered electrochemical processes with very low power consumption and pollution.

2. Results and Discussion

The system is composed of an R-TENG and an electrochemical unit for wastewater treatment. The R-TENG holds a multilayered structure, which consists of mainly two parts: a rotator and a stator with two acrylic sheets as supporting substrates, as shown in **Figure 1**a. The core parts of the rotator and stator are both print circuit boards (PCBs) covered by arrayed copper sectors with a central angle and length of 1° and 60 mm on substrate of underlying epoxy glass cloth laminate sheet (FR4). The different thing is that the pattern for radially arrayed sectors on rotator-PCB (top PCB) is identical, while the patterns for arrayed sectors on stator PCB (bottom PCB) are two complementary structures. The two kinds of complementary arrayed sectors are disconnected by fine trenches in between and each kind of sectors is mutually connected at one end. On the supporting substrate of the rotator, the top PCB was adhered acting as a contact-triboelectrification layer. On the supporting substrate of the stator, a foam layer, a bottom PCB layer, and a Kapton triboelectrification layer were pasted together sequentially from top to bottom. The Kapton layer (50 μm) works as another triboelectrification surface. The bottom PCB layer, also named copper grating electrodes layer, is mainly working as output electrodes. The foam layer that ensures intimate contact between two triboelectrification layers acts as a buffer. Since the miniaturizing and integrating of electrodes, the TENG takes the advantage of a relatively high current. As presented in Figure 1b,c, under 450 revolutions per minute (rpm), the short-circuit current (I_{sc}) has an average amplitude of 1.5 mA (Figure 1b), and the open-circuit voltage (V_{oc}) holds a peak value around 150 V (Figure 1c). What's more, as can be seen through Figure 1b,c, the continuous AC output oscillates at an approximate frequency of 1600.

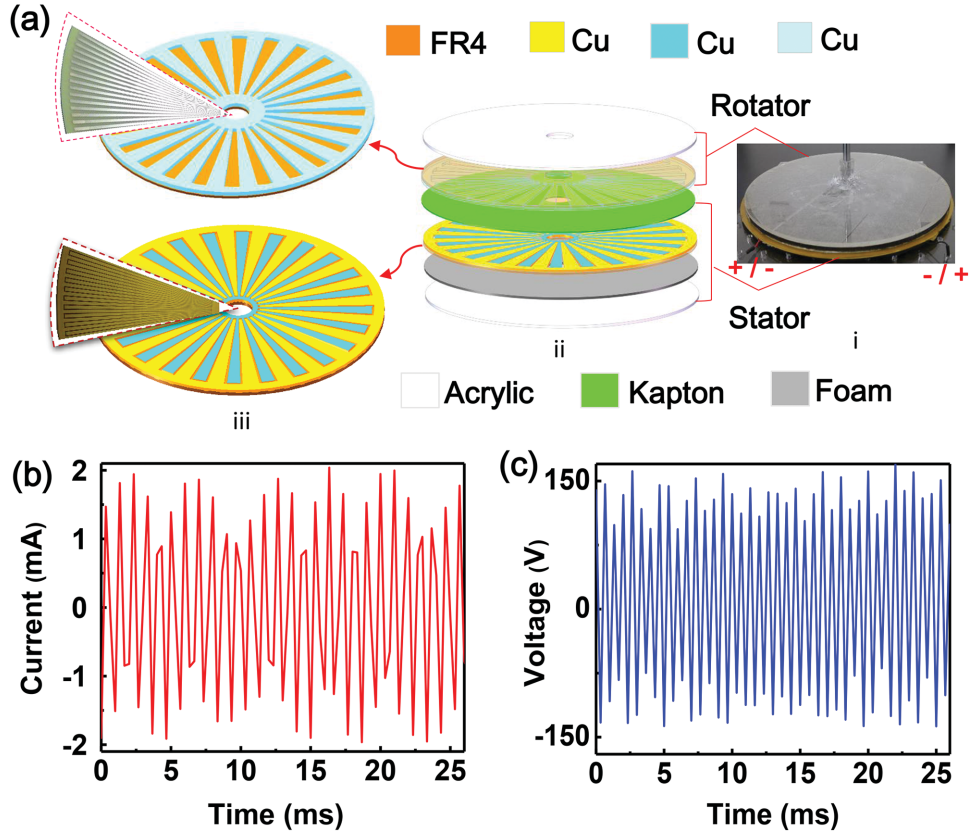

Figure 1. Structural design and characterizations of the R-TENG. a) Illustrations of the R- TENG. (i) the optical image and (ii) the schematic exploded view of the R-TENG which consists of a rotator and a stator. (iii) PCB patterns of the rotator and stator; inserts are the sectional optical images of PCBs. b) The short-circuit current and c) the open-circuit voltage of the as-fabricated R-TENG when rotating speed is about 450 rpm.

A detailed description of its generation mechanism is presented in the following working principle section.

Simply speaking, the power generation principle of a TENG is based on the collaboration of triboelectrification and electrostatic induction. During the rotation process, the Kapton film layer and the top PCB triboelectrification layer are configured to match for a full contact and good tribioelectrification. Because of different triboelectric polarities of the two triboelectric surfaces, positive and negative electric charges are created on the copper surface and Kapton surface respectively after a little while of friction, as illustrated in the longitudinal cross-sectional view defined by an arbitrary intersection in **Figure 2**a. When two electrodes in bottom are connected, free charges can redistribute between electrodes through the cyclic departure and approach of two micro-triboelectric unit, resulting in electric potential difference and current. The initial state (Figure 2a-i) corresponds to the maximum V_{oc} for the biggest the electric potential difference. When the rotator spins to the state of Figure 2a-ii, the voltage diminishes to zero. In the final state (Figure 2a-iii), the voltage reaches the maximum V_{oc} in reverse. Further rotation beyond the final state, V_{oc} changes in a reversed way.

To investigate the influence of the rotating speed on the performance of R-TENG, we changed the rotating speed of R-TENG from 150 to 650 rpm. As demonstrated in Figure 2b, when the

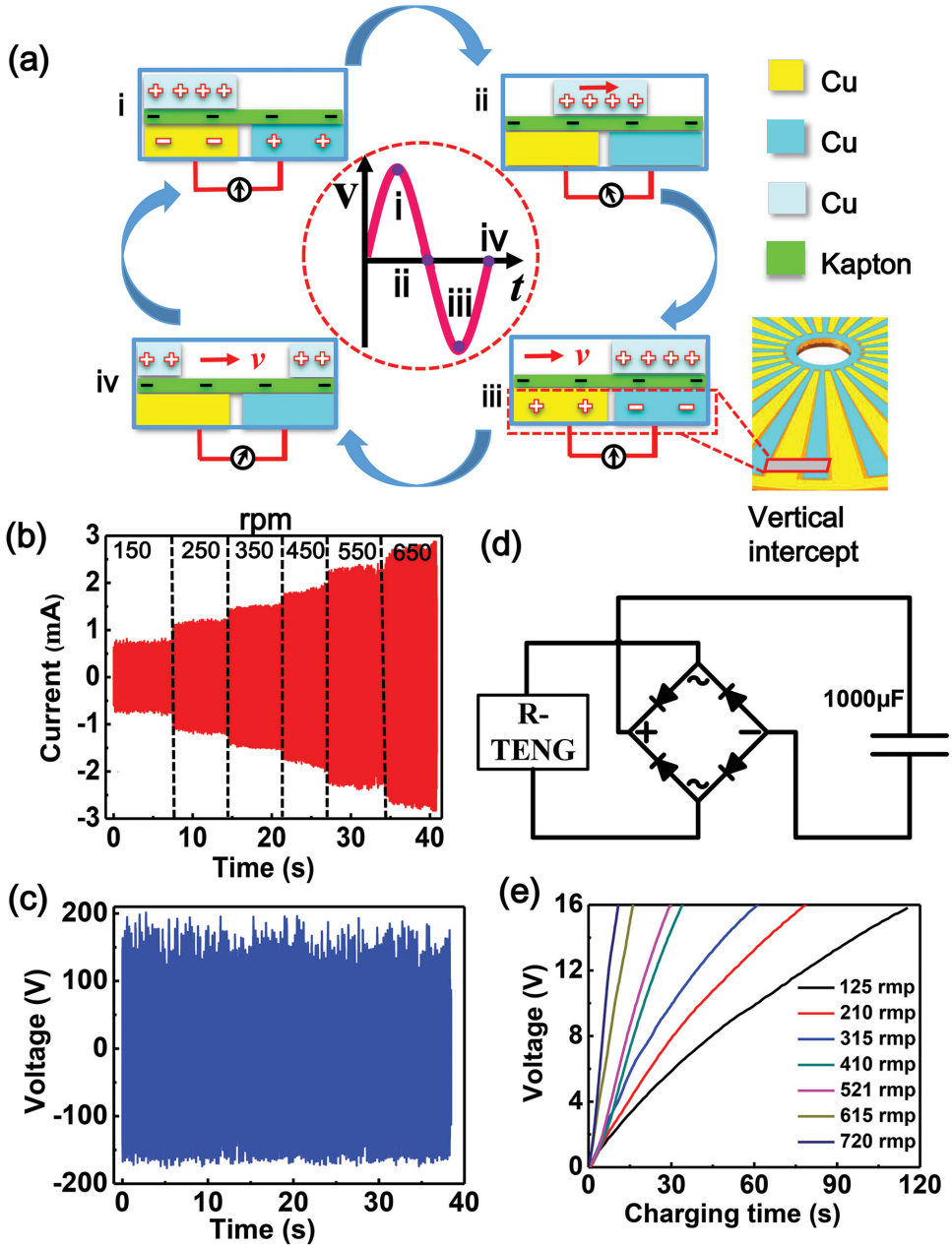

Figure 2. Working mechanism of the R-TENG and the influence of rotating speed on the output of R-TENG. a) The working mechanism of R-TENG. b) Short-circuit current of R-TENG at different rotation rates. c) Open-circuit voltage of the TENG at different rotation rates. d) The working circuit of R-TENG charging a capacitor. e) Charging time of a 1000 μF capacitor to 16 V when charged by the R-TENG.

rotating speed was 150 rpm, the current was about 0.8 mA. With the speed rising to 650 rpm, the current increased up to 2.85 mA. However, the voltage remained at a peak value of 180 V (Figure 2c). The current is increasingly proportional to the rotating speed, while the voltage output is not affected by it. We also tested its capacity for charging a 1000 μF capacitor. Its working circuit is shown in Figure 2d, that is, the output of R-TENG must be tuned into unidirectional current by rectifying bridge before charging a capacitor. From Figure 2e, we can see that the higher the rotation speed of R-TENG, the shorter is the charging time of capacitor. This result is very accordant with Figure 2b.

After looking into the R-TENG performance influence, a further step was taken to evaluate the performance of the self-powered wastewater treatment system for RhB and copper removal. Prior to the measurement of its performance, we firstly introduced the self-powered wastewater treatment system and its treating mechanism. The system is mainly an electrochemical unit, which includes three parts: power resource, electrodes and electrolyte, as shown in **Figure 3**a,b. Because of its inertia, low-cost, and effectiveness, commercially available graphite rod was selected as anode. Considering the high capacity for recovering copper, iron plate was selected as cathode. Electrodes were kept

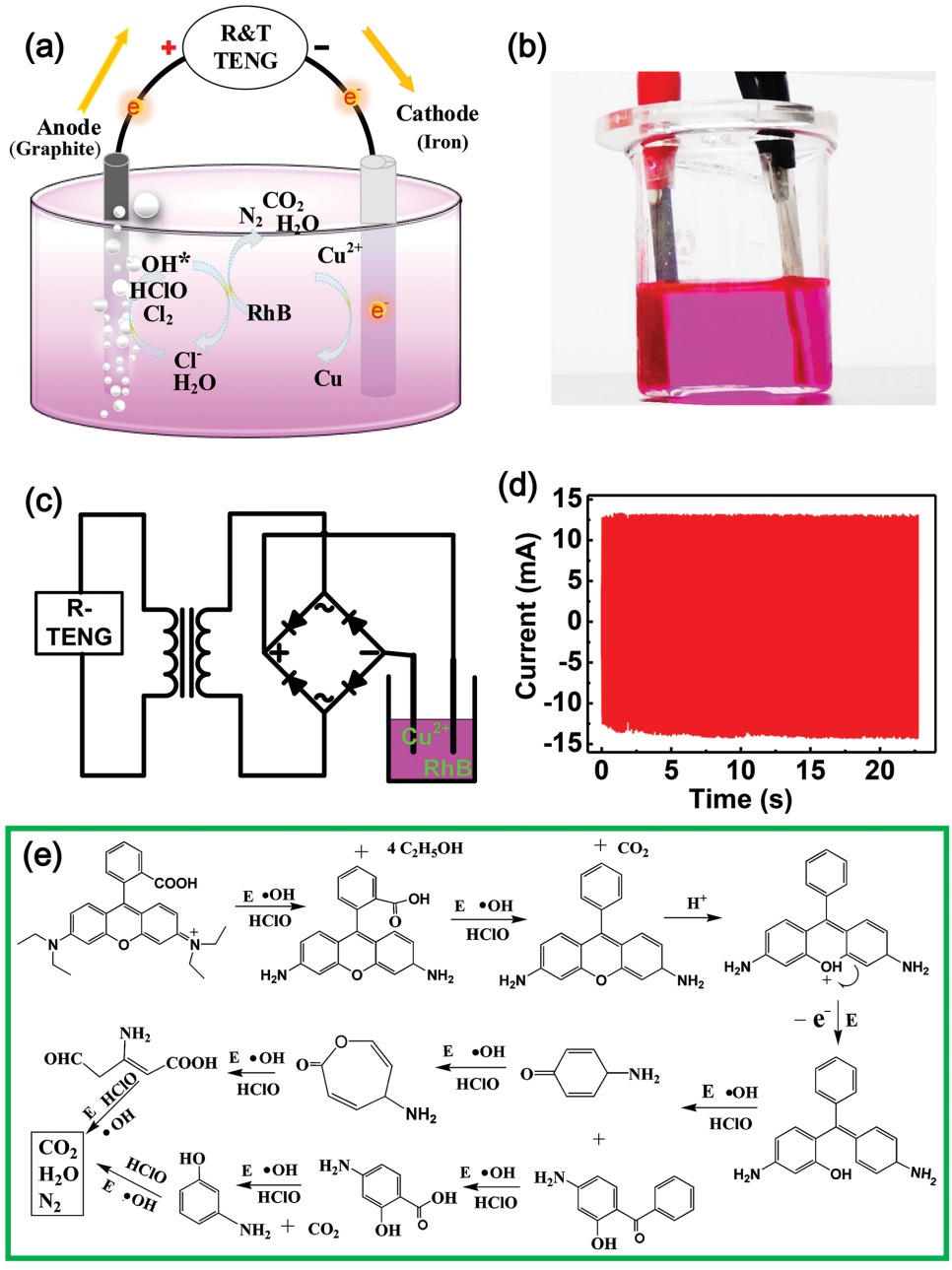

Figure 3. Experimental setup for removing Cu^{2+} and RhB. a) Schematic diagram of the Cu^{2+} and RhB removing powered by transformed and rectified TENG (R&T TENG). b) Optical image of the electrochemical unit for Cu^{2+} and RhB removal. c) The electric circuit diagram of the wastewater treatment system. d) The short-circuit current after transformation. e) The proposed degradation process of RhB.

vertically and parallel to each other at an inner electrode distance of 3 cm. 20% (w/v) NaCl solution was chosen as electrolyte to improve the ionic strength of solution and the RhB removal. To drive the reactions on electrodes for removing RhB and Cu^{2+}, the above R-TENG is transformed and rectified (corresponding transforming and rectifying circuit is shown in Figure 3c) as a power source, for the reason that the conventional transformer could boost the output current and reduce the output voltage,[12,16] and that the rectifier could change the continuous AC output into an unidirectional pulse signal. When rotation rate is about 450 rpm, after transformation, the current of 1.8 mA was enhanced up to 12.5 mA (Figure 3d), while the voltage of 150 V was reduced to about 13 V (Figure 1, Supporting Information). Then the transformed and rectified R-TENG (R&T R-TENG) is connected with the sewage treatment system as a power source. The dynamic current and voltage for wastewater treatment can be found in Movie S1 in the Supporting Information.

According to the electrochemical principles of electrolysis, the working mechanism of the advanced electrochemical treatment of RhB and Cu^{2+} are proposed as follows

At anode

$$2H_2O \rightarrow 2OH^* + 2H + 2e^- \quad (1)$$

$$Cl^- + H_2O \rightarrow ClO^- + 2H^+ + 2e^- \quad (2)$$

$$OH^* + RhB \rightarrow CO_2\uparrow + N_2\uparrow + H_2O \quad (3)$$

$$H^+ + ClO^- + RhB \rightarrow CO_2\uparrow + N_2\uparrow + Cl^- + H_2O \quad (4)$$

At cathode

$$Cu^{2+} + 2e^- \rightarrow Cu \quad (5)$$

Other reactions

$$Fe + Cu^{2+} = Fe^{2+} + Cu \quad (6)$$

$$2H^+ + 2Fe^{2+} + ClO^- = 2Fe^{3+} + Cl^- + H_2O \quad (7)$$

$$Fe^{3+} + e^- = Fe^{2+} \quad (8)$$

$$Fe^{2+} + 2e^- = Fe \quad (9)$$

Firstly, H_2O and Cl^- were transferred to graphite electrode (anode) for the discharge reaction of anode, resulting in the formation of super-oxidative hydroxyl radical OH* and ClO^- (Equations (1) and (2)). Then the oxidative species degrade RhB completely into small molecules like CO_2, H_2O, N_2, etc. (Equations (3) and (4)) when oxidative species are excessive. If RhB is at a very high concentration, RhB may be incompletely degraded into smaller molecules without enough oxidative species. The proposed complete degrading process of RhB is illustrated in Figure 3e through series of parallel and consecutive reactions. To prove the reliability of this degradation process, we tested the Fourier transform infrared spectrum (FTIR), liquid chromatography (LC) and mass spectroscopy (MS) of the sample before and after degradation (more details are shown in Figure 2 in the Supporting Information). As shown in Figure 2a in the Supporting Information, before degradation, there are peaks at 1692, 1643, 1583, 1548, 1469, 1336, 1174, 1122, and 1072 cm^{-1}. The 1692 cm^{-1} peak corresponds to C = O stretch of carboxyl group and 1643 cm^{-1} peak is caused by –C = C– stretch. Peaks at 1583, 1548, and 1469 cm^{-1} are the characteristic infrared (IR) absorption of aromatic ring. The absorbance at 1336 and 1122 cm^{-1} is caused by stretching vibration of Ar—N and C—N, and the absorbance at 1174, 1072 cm^{-1} belongs to =C—O—C. After an hour of degradation, many absorption peaks have vanished and a very wide absorption peak in the range of 1600–1700 cm^{-1} appears, depicting the breakage of the RhB structure and the generation of carboxylic acids. At the cathode, copper ions seized electrons and turned into deposited copper (Equation (5)). Because of the high activity of iron cathode, copper ions also could be reduced into elementary copper directly, resulting in the generation of ferrous ions (Equation (6)). Through a series of electrochemical reactions (Equations (7)–(9)), the ferrous ions are reduced into iron again at the cathode, realizing the cyclic utilization of the iron. Here, the ferrous ions act as catalyst for the reduction of copper ions, which will be discussed at length later. The advanced electrochemical wastewater treatment is very similar to electro-Fenton method with electro-generated H_2O_2 and Fe^{2+}, but no oxygen is bubbled.

For the sake of simplicity and controllability, the performance of the wastewater treatment system was preliminarily evaluated through a motor driven R-TENG at a fixed rotating speed of 600 rpm. After transforming and rectifying the output of R-TENG, the current in the circuit could high up to 13 mA and takes on a feature of cyclical punctuation, as shown in **Figure 4**a. The voltage across the electrochemical unit also fluctuates around 3 V in a pulse-mode (Figure 4b). The concentration of RhB and Cu(II) was evaluated by ultraviolet absorption spectroscopy method for several advantages such as cost-effectiveness, easy operation, and high sensitivity. On one hand, RhB solution and Cu(II)-Neocuproine (Cu^{2+}-NCP) complexes have different maximum absorbance at 454[17] and 552 nm[18] respectively; On the other hand, the co-existence of Cu^{2+} or Cu(II)-NCP or RhB has no effect on the detection of each other, as shown in Figure 3 in the Supporting Information. Thus RhB and Cu(II) concentration could be determined simultaneously. The detailed characterization of Cu^{2+} concentration is demonstrated in experimental part.

In order to validate the decrease of RhB and Cu^{2+}-NCP absorption peak intensity is attributed to the electrochemical degradation, a control experiment was conducted without triboelectrification or external power sources. The UV–visible curve of the RhB and Cu^{2+}-NCP remained unchanged as the time passed by (Figure 4, Supporting Information), indicating electricity is a must for the electrochemical degradation. Without electricity, RhB and Cu^{2+} cannot decrease on its own over time. After electrolysis of 3 h, the removal efficiency of RhB and Cu^{2+} could reach 100% and 97.3% (Figure 4c) respectively with initial concentration about 300 and 150 ppm respectively, indicating the effectiveness of the wastewater treatment system using R-TENG. The quicker color change of the wastewater with a low concentration of RhB can be seen through Movies S2 and S3 in the Supporting Information. From Figure 4c, we also could see that Cu^{2+} is more refractory compared with RhB, as may

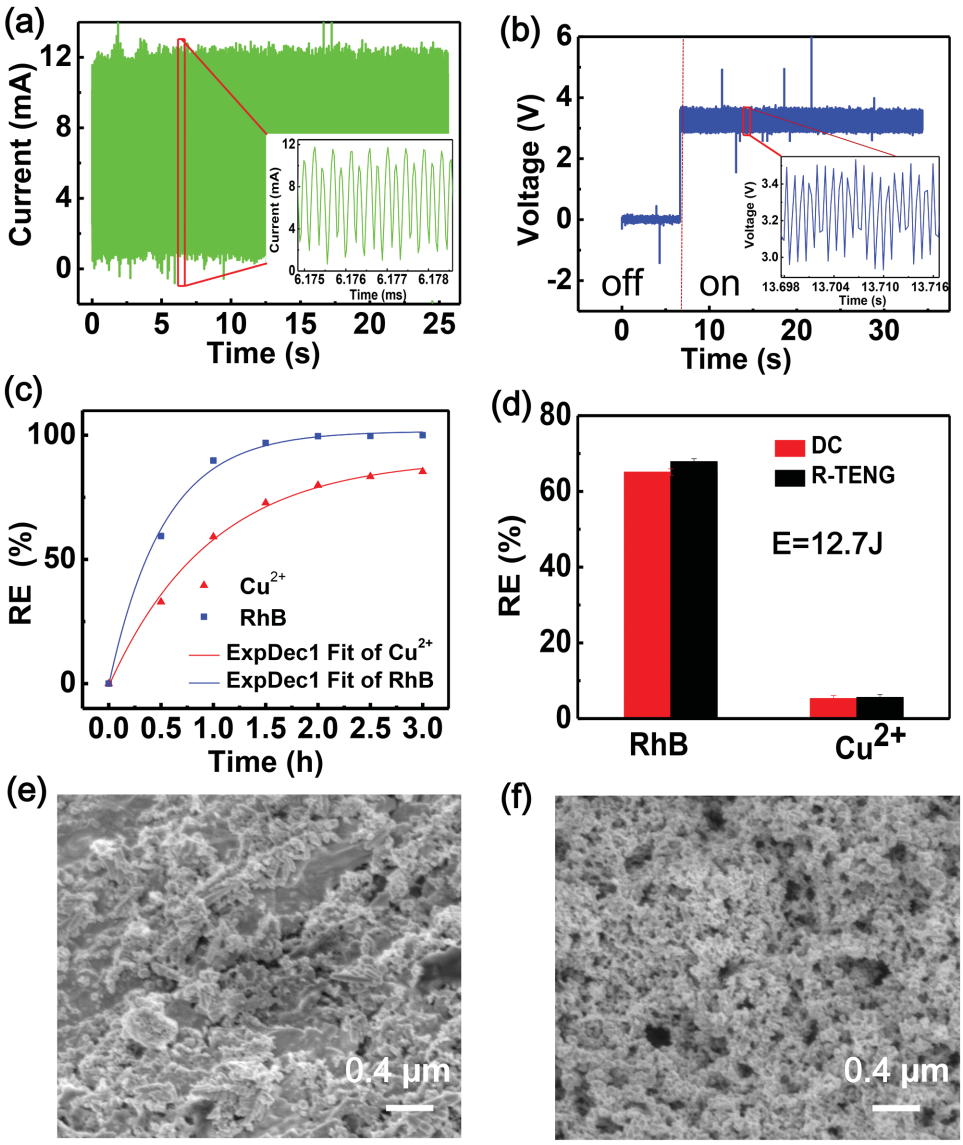

Figure 4. a) Current in the circuit of the wastewater treatment system. Inset: enlarged view of the current feature. b) Voltage across the electrochemical unit before and after the motor is turned on. Inset: enlarged view of the voltage feature. c) RE of RhB and Cu^{2+} after 3 h. d) Comparison of performances of the system when driven by DC supply and R-TENG with the same energy consumption. The morphology of the deposited copper on silver wire surface when the system is driven by e) DC supply and f) R-TENG.

be explained by the reason that the super-oxidative active species is relatively more stable than $Fe^{2+}$and prompt the degradation of RhB, while the Fe^{2+} is quickly oxidized to Fe^{3+} and soon loses its catalysis ability for Cu^{2+}. It is also worth noting that the removal efficiencies of RhB and Cu^{2+} change rapidly at first and then gradually become slower. Furthermore, the relationship between concentration and time approximately accords with pseudo-first-order kinetics equation

$$\ln\left(\frac{C_t}{C_0}\right) = -k_a t \text{ or } C_t = C_0 \times e^{-k_a t}$$

where k_a represents the apparent first order rate constant, C_0 is the initial concentration of substrate, C_t is concentration after given time t.

We also compared the performances of the system driven by DC supply and R-TENG. At the same condition, when total energy consumption is 12.7 J, the removal efficiencies of RhB and Cu^{2+} with R-TENG supply are a little bit higher than those with DC supply, as shown in Figure 4d. This is due to the electrolysis (10 min) with R-TENG is longer than those (7.6 min) with DC supply when consuming equal energy, which contributes to better coagulation and adsorption. Moreover, the current peak valley of the R-TENG output provides sufficient time for substance migration, also promoting the reactions. For testing the capability of the system for electroplating, we changed the cathode into silver wire. Through the morphology comparison of the deposited copper on silver (Figure 4e,f), we could see that the copper deposited on the cathode through R-TENG is much denser, more uniform, and with smaller grain size (d = 20 nm)

than those produced by DC process, which is very promising in electroplating industry.

A systematic investigation of factors, particularly electrodes, electrolytes, concentration of electrolytes and the initial concentration of pollutants, were made to comprehensively evaluate the performances of RhB and Cu^{2+} removal based on R-TENG with speeding rate of 600 rpm, electrode working distance of 4 cm, and electrode area of 5 cm^2. From **Figure 5**a, we could learn that the removal efficiency of RhB and Cu^{2+} with iron cathode is higher than those with stainless steel and copper plate. The reason for bad performance of copper plate is the dissolution reactions of copper in chloride solution.[19] While the better performance of iron plate than stainless steel is due to the generation of ferrous ions, which is verified by Figure 5 in the Supporting Information, showing the addition of ferrous ions is good for the removal of copper ions. In order to access the role of different electrolytes in the sewage treatment system, experiments were also performed in different solutions, including 16% (w/v) NaCl, 16% (w/v) Na_2SO_4, and deionized water. The result is shown in Figure 5b, depicting the addition of electrolytes is good for waste removal, particularly NaCl. Moreover the higher the mass concentration of NaCl is (Figure 5c), the better removal efficiency is, which is due to the higher electric conductivity and lower resistance. Figure 5c shows the lower pH

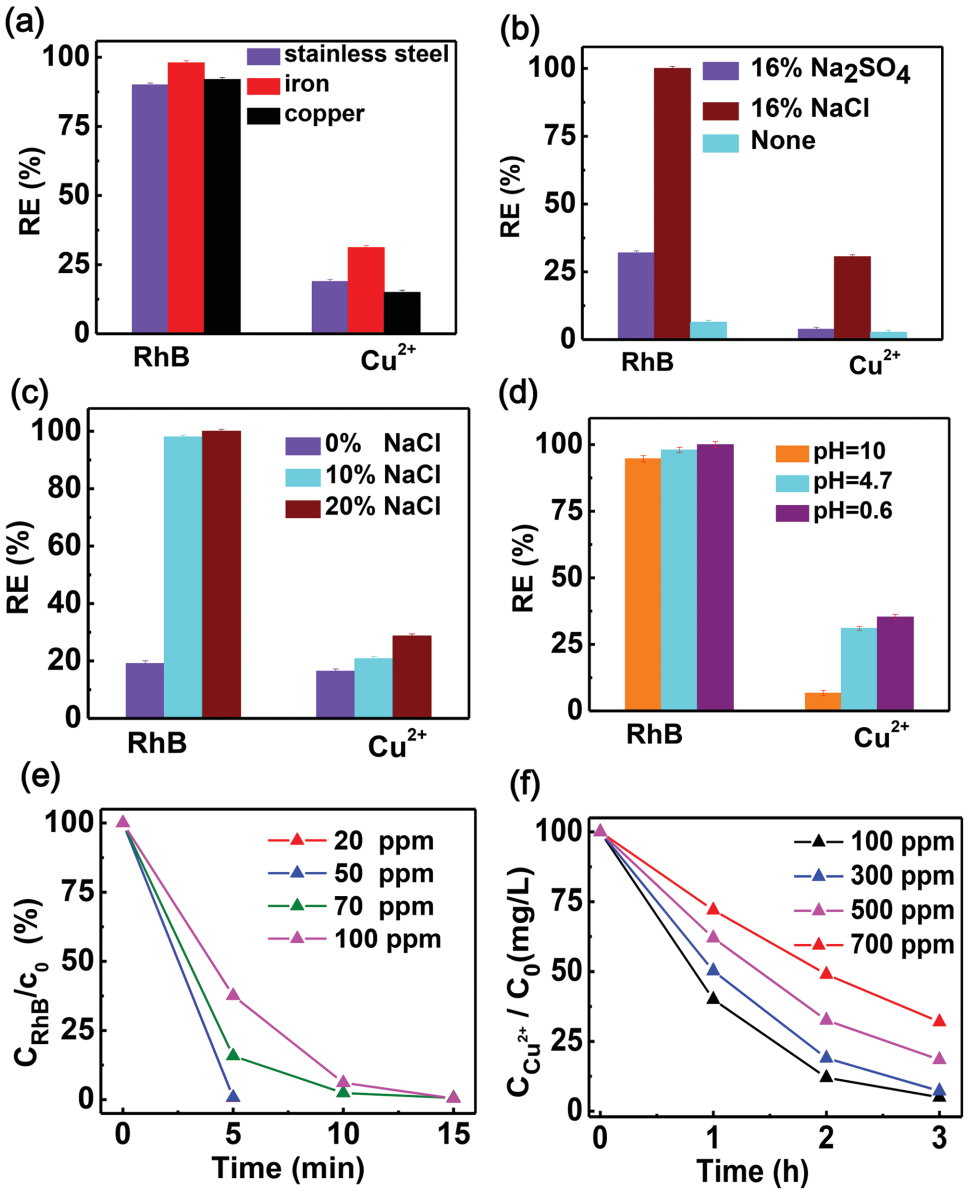

Figure 5. Factors affecting Cu^{2+} and RhB removal. The influence of a) different cathode, b) different electrolyte, c) different electrolyte concentration, d) different pH, and d) different initial concentration of e) RhB and f) Cu^{2+} on the removal of RhB and Cu^{2+}. R-TENG rotation rate, 600 rpm; electrode distance, about 3 cm; effective anode and cathode area are about 2 and 5 cm^2 respectively. For (a–d), initial concentrations of Cu^{2+} and RhB are 300 and 150 ppm respectively, and electrolysis time is 20 min. For (e,f), the pH is 0.6 without adding any acid or base, and the electrolyte concentration of NaCl is 20%.

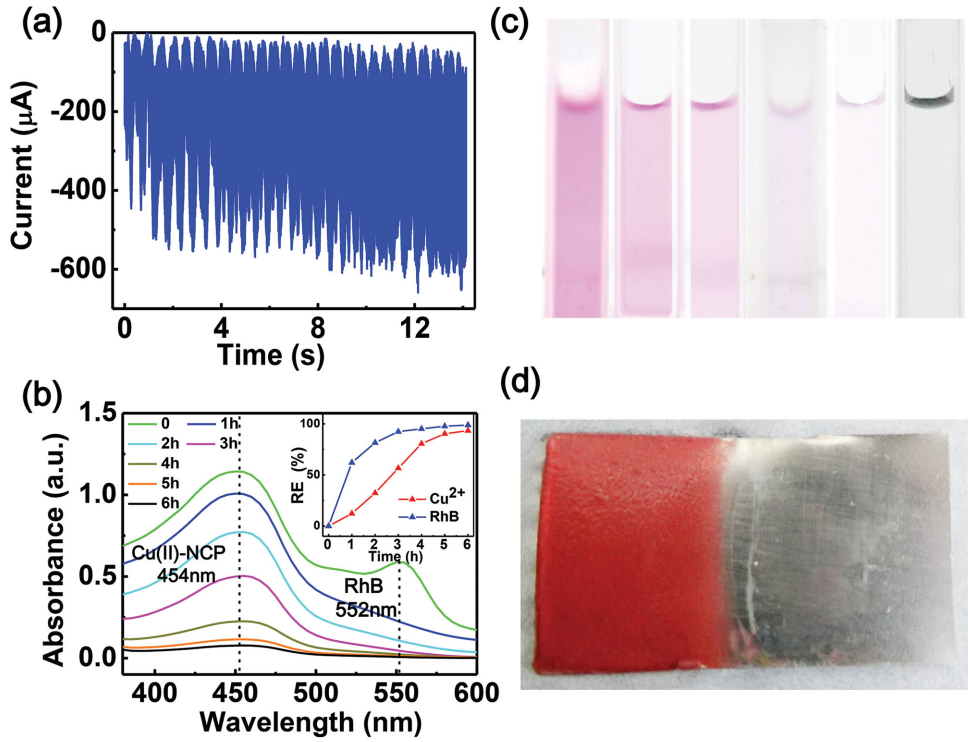

Figure 6. Demonstrations of wastewater treatment system driven by water-driven R-TENG. a) The current in the circuit of the wastewater treatment system. b) UV–visible absorption spectra of the Cu^{2+}-NCP and RhB samples with diluted multiples of 25 for the different working times. Insert: corresponding removal efficiency of Cu^{2+} and RhB for different working times. c) Corresponding color change of the sample solution in (b). d) The optical image of the iron plate after deposition of copper. Water landing speed is 1.6 $m \cdot s^{-1}$; pH is 0.6; electrode distance, about 3 cm; NaCl electrolyte concentration, 20%. Effective anode and cathode area are about 2 and 5 cm^2 respectively.

benefits RhB and Cu^{2+} removal. When the initial concentration of RhB and Cu^{2+} changed, the degrading time and removal efficiency also changed (Figure 5e,f). For RhB under 100 ppm, the time of complete degradation is just for 15 min. For Cu^{2+} under 300 ppm, after 3 h, the residual concentration could down to 4.6%, which means 95.4% of copper ions are removed.

From the experiments above, we could see that the system shows good performance for treating RhB and Cu^{2+}. In order to make the wastewater treatment system work in a self-powered manner without using an external power source, we also investigated the performance of the wastewater treatment system using the electricity harvested from water itself under laboratory conditions. To drive the R-TENG rotates, a water-wheel is coaxially connected, as illustrated in Figure 6, Supporting Information. The water velocity impacting the R-TENG is about 1.6 $m \cdot s^{-1}$ and provided by a pumper (volume flow rate is 3 $m^3 \cdot h^{-1}$). At this condition, the current in the circuit is about 0.4 mA (**Figure 6**a). With the proceeding of the electrolysis, the absorption peak intensity of RhB and Cu^{2+} goes down gradually and the color gets dimer and dimer, as shown in Figure 6b,c respectively. After 6 h of electrolysis, the absorbance of RhB and Cu^{2+} with diluted multiples of 25 reduces from 1.13 to 0.08, and from 1.14 to 0.07 respectively, corresponding removal efficiency high up to 98.8% and 93.4% respectively. Figure 6d shows the iron cathode after deposition of copper for 3 h. Thus, the sustainable wastewater treatment system shows good performance in laboratory conditions, and the performance is expected to be much better under real strong water flow.

3. Conclusion

In conclusion, by harvesting the flowing kinetic energy of water using an R-TENG, we demonstrated a self-powered wastewater treatment system that simultaneously removes RhB and copper ions through an advanced electrochemical unit. With the electricity generated by R-TENG, the system has a very good removal capacity of RhB with removal efficiency approximately of 100% just within 15 min when the initial concentration of RhB is around 100 pp at an optimized condition. Though the copper removal is a little difficult and slower, the efficiency also could high up to 97.3% after 3 h within an initial concentration of 150 ppm at an optimized condition. Importantly, the system exhibited better performance for waste removing using the pulsed output of R-TENG than those using DC supply when consuming equal amount of energy. The copper layer deposited on silver cathode through R-TENG are much denser, more uniform and with smaller grain size (d = 20 nm) than those produced by DC supply, which also hints very promising applications of the R-TENG in electroplating industry. With a collection of compelling features, such as high removal efficiency for RhB and copper ions, feasibility on organic pollutants with low contamination, extremely low cost, simplicity, and reusability, the presented work not only provides a new and efficient pathway for sustainable wastewater treatment, but also provides access to other self-powered electrochemical processes with very low power consumption and pollution.

4. Experimental Section

Fabrication of R-TENG: Stator: (1) Cut a square-shaped acrylic sheet as a substrate with a dimension of 20 cm by 20 cm by 3 mm by using a laser cutter; (2) Drill holes on four corners of the substrate, then fix the substrate on a flat stage by screws; (3) Adhere a layer of foam on the substrate as a buffer; (4) Stick a prepared commercialized PCB above the foam. The PCB has complementary and separated gratings which act as electrodes; (5) Adhere a thin layer of Kapton (50 μm) onto the PCB. Rotator: (1) Cut a through-hole in the center of a disc-shaped acrylic substrate (diameter, 15cm; thickness, 3mm) by using a laser cutter. (2) Stick another prepared commercialized PCB on the substrate. The PCB has a collection of radially arrayed sectors with a central angle of 1°. Lastly, for fabricating the R-TENG, the stator and rotator are put together with an axle bar and a bearing.

Experiment of Cu^{2+} and RhB Removal: Without special illustration, all the experiments for treating Cu^{2+} and RhB was performed in a 50 mL breaker containing 25 mL sample solution of $CuSO_4$ and RhB, cylindrical graphite cathode and iron anode at ambient temperature without adjusting pH. Before all the experiments, electrodes were washed neatly using distilled water. During the treatment, electrodes were kept vertically and parallel to each other. Electrode distance was about 3 cm; effective anode area was 2 cm^2, effective cathode area was about 5 cm^2, concentration of NaCl electrolyte was 20% (m/v). The output of R-TENG was transformed and rectified to peak current about 13 mA with rotation rate around 600 rpm for waste removal. Samples were collected at regular interval to find the residual concentration of RhB and Cu^{2+}. The removal efficiency was determined by following equation

$$\text{Removal efficiency } \eta(\%) = \frac{C_0 - C_t}{C_0} \times 100\%$$

where C_0 and C_t are RhB or Cu^{2+} concentrations at initial condition ($t = 0$) and after the specific time t.

Determination of RhB and Cu^{2+} Concentration: The concentration of RhB and Cu^{2+} was measured by UV–vis–NIR spectrophotometer (UV-3600, Shimadzu, Japan). RhB could be monitored directly at the peak wavelength of 552 nm. For Cu(II) determination, 2,9-Dimethyl-1.10-phenanthroline ("neocuproine") solution (0.2% m/v, 500 mL) as a chromogenic reagent of Cu^{2+} was firstly prepared. Then the collected sample (0.5 mL) was sequentially added with 1.5 mL hydroxylamine hydrochloride (10% m/v), 3 mL EDTA-Na_2EDTA buffer (pH = 5.7), 3 mL sodium citrate (37.5% m/v), and 1.5 mL neocuproine (0.2% m/v). After that, the mixture was ultrasonically shaken for 2 min to ensure sufficient complexation reaction, and then diluted to 25 mL water for UV–vis–NIR spectrophotometer, and the Cu-NCP has an absorbance peak at 454 nm.

Supporting Information

Supporting Information is available from the Wiley Online Library or from the author.

Acknowledgements

S.W.C. and N.W. contributed equally to this work. The authors thank the financial support from the National Natural Science Foundation of China (NSFC Nos. 21475008, 21275017, 21127007, 21173017, 51272011, and 21275102), the Program for New Century Excellent Talents in University (NCET-12-0610), the science and technology research projects from the education ministry (213002A), National "Twelfth Five-Year" Plan for Science & Technology Support (No. 2013BAK12B06), the "thousands talents" program for pioneer researcher and his innovation team, China, National Natural Science Foundation of China (Grant No. 51432005; No. Y4YR011001).

Received: September 6, 2015
Revised: November 10, 2015
Published online: February 8, 2016

[1] a) I. Rafiqul, C. Weber, B. Lehmann, A. Voss, *Energy* **2005**, *30*, 2487; b) M. A. Shannon, P. W. Bohn, M. Elimelech, J. G. Georgiadis, B. J. Marinas, A. M. Mayes, *Nature* **2008**, *452*, 301; c) P. Zakkour, M. Gaterell, P. Griffin, R. Gochin, J. Lester, *J. Environ. Manage.* **2002**, *66*, 115; d) I. Karlsson, *Water Sci. Technol.* **1996**, *34*, 203.

[2] S. T. Oh, J. R. Kim, G. C. Premier, T. H. Lee, C. Kim, W. T. Sloan, *Biotechnol. Adv.* **2010**, *28*, 871.

[3] a) J. J. Pignatello, E. Oliveros, A. MacKay, *Crit. Rev. Env. Sci. Tecnol.* **2006**, *36*, 1; b) M. N. Chong, B. Jin, C. W. K. Chow, C. Saint, *Water Res.* **2010**, *44*, 2997.

[4] W.-W. Li, H.-Q. Yu, Z. He, *Energy Environ. Sci.* **2014**, *7*, 911.

[5] a) C. Forrestal, P. Xu, Z. Ren, *Energy Environ. Sci.* **2012**, *5*, 7161; b) B. E. Logan, K. Rabaey, *Science* **2012**, *337*, 686.

[6] a) Y. L. Pang, A. Z. Abdullah, S. Bhatia, *Desalination* **2011**, *277*, 1; b) D. Mohan, C. U. PittmanJr, *J. Hazard Mater.* **2007**, *142*, 1; c) C. T. Wang, W. L. Chou, Y. M. Kuo, *J. Hazard Mater.* **2009**, *164*, 81; d) M. Y. A. Mollah, P. Morkovsky, J. A. G. Gomes, M. Kesmez, J. Parga, D. L. Cocke, *J. Hazard Mater.* **2004**, *114*, 199.

[7] M. C. Cammarota, D. M. G. Freire, *Bioresour. Technol.* **2006**, *97*, 2195.

[8] a) G. H. Chen, *Sep. Purif. Technol.* **2004**, *38*, 11; b) C. A. Martinez-Huitle, E. Brillas, *Appl. Catal. B-Environ.* **2009**, *87*, 105; c) C. A. Martinez-Huitle, S. Ferro, *Chem. Soc. Rev.* **2006**, *35*, 1324.

[9] G. Chen, *Sep. Purif. Technol.* **2004**, *38*, 11.

[10] M. Schlesinger, M. Paunovic, *Modern Electroplating*, *55*, **2011**, John Wiley & Sons, Hoboken, NJ, USA **2011**.

[11] a) X. W. Liu, X. F. Sun, Y. X. Huang, G. P. Sheng, S. G. Wang, H. Q. Yu, *Energy Environ. Sci.* **2011**, *4*, 1422; b) B. Logan, S. Cheng, V. Watson, G. Estadt, *Environ. Sci. Technol.* **2007**, *41*, 3341; c) H. Liu, R. Ramnarayanan, B. E. Logan, *Environ. Sci. Technol.* **2004**, *38*, 2281; d) Y. F. Zhang, J. S. Noori, I. Angelidaki, *Energy Environ. Sci.* **2011**, *4*, 4340.

[12] W. Tang, Y. Han, C. B. Han, C. Z. Gao, X. Cao, Z. L. Wang, *Adv. Mater.* **2015**, *27*, 272.

[13] Q. Jiang, Y. Han, W. Tang, H. Zhu, C. Gao, S. Chen, M. Willander, X. Cao, Z. L. Wang, *Nano Energy* **2015**, *15*, 266.

[14] S. Chen, C. Gao, W. Tang, H. Zhu, Y. Han, Q. Jiang, T. Li, X. Cao, Z. Wang, *Nano Energy* **2014**, *14*, 217.

[15] a) G. Cheng, Z. H. Lin, Z. L. Du, Z. L. Wang, *ACS Nano* **2014**, *8*, 1932; b) Z. H. Lin, G. Cheng, W. Z. Wu, K. C. Pradel, Z. L. Wang, *ACS Nano* **2014**, *8*, 6440; c) X. N. Wen, W. Q. Yang, Q. S. Jing, Z. L. Wang, *ACS Nano* **2014**, *8*, 7405; d) G. Zhu, Y. Su, P. Bai, J. Chen, Q. Jing, W. Yang, Z. L. Wang, *ACS Nano* **2014**, *8*, 6031; e) Z. H. Lin, G. Cheng, S. Lee, K. C. Pradel, Z. L. Wang, *Adv. Mater.* **2014**, *26*, 4690.

[16] G. Zhu, J. Chen, T. Zhang, Q. Jing, Z. L. Wang, *Nat. Commun.* **2014**, *5*, 3426.

[17] Y. Zhang, Y. Fang, L. J. Yu, *Non-Ferrous Min. Metall.* **2001**, *1*, 012.

[18] N. Daneshvar, M. A. Behnajady, M. K. A. Mohammadi, M. S. S. Dorraji, *Desalination* **2008**, *230*, 16.

[19] a) T.-C. Chen, R. Priambodo, R.-L. Huang, Y.-H. Huang, *J. Waste Manage.* **2013**; b) E.-Y. Kim, M.-S. Kim, J.-C. Lee, M. K. Jha, K. Yoo, J. Jeong, *Miner. Eng.* **2008**, *21*, 121.

